LLNL-JRNL-2008837

Lawrence Livermore National Laboratory

Modeling the influence of the solid electrolyte interphase on the sand's time and dendrite formation on lithium metal electrodes

T Roy, H Li, G Bucci, C Orme, N Brady, S Selvasundarasekar, V Ehlinger, R Akolkar, N Cross, T Lin

February 2026

Discover Electrochemistry

Disclaimer

This work performed under the auspices of the U.S. Department of Energy by Lawrence Livermore National Laboratory under Contract DE-AC52-07NA27344.

Discover Electrochemistry

RESEARCH Open Access

Modeling the influence of the solid electrolyte interphase on the sand's time and dendrite formation on lithium metal electrodes

Nicholas R. Cross[1], Tiras Y. Lin[1], Nicholas W. Brady[1], Sam Sankar Selvasundarasekar[2], Victoria M. Ehlinger[1], Thomas Roy[1], Hanyu Li[1], Rohan Akolkar[2], Marcus A. Worsley[1], Christine Orme[1] and Giovanna Bucci[1*]

*Correspondence:
Giovanna Bucci
bucci3@llnl.gov
[1]Lawrence Livermore National Laboratory, 7000 East Ave, Livermore, CA 94550, USA
[2]Department of Chemical and Biomolecular Engineering, Case Western Reserve University, Cleveland, OH 44106, USA

Abstract

Lithium metal is a sought after battery material for its high energy density due to the low electrochemical potential and density. However, lithium metal is also highly reactive, which results in a strong propensity for dendrite formation. The Sand's time has previously been used to predict the time of dendrite initiation on metals that do not form a solid-electrolyte interphase (SEI), but it has been shown that the Sand's time is not accurate for lithium electrodes when using transport parameters associated with the electrolyte. Thus, we built a numerical model to simulate lithium ion transport through a growing SEI to predict the Sand's time. The numerical model is shown to be more accurate than previous analytical solutions, especially for low current densities. We then analyze the sensitivity of the Sand's time to different SEI properties and the chemical potential gradients present in the SEI, driving lithium transport. The results showed that high lithium concentration has a greater impact at high current density, while fast diffusivity is more important at low current density. Lastly, we modeled the influence of surface roughness on the plating evolution and chemical potential gradients when an SEI is present in comparison to the electrolyte. As a result, we demonstrate that the SEI plays a critical role in lithium electrode stability, and that improved characterization techniques are needed to better understand transport through the SEI and increase lithium metal utilization in energy storage devices.

1 Introduction

With the conversion to an electrified society, advances in energy storage technologies will be needed to power mobile devices and store excess renewable energy. [1] Lithium metal is a highly attractive material because it has high charge capacity (3860 mAh g^{-1}), low electrochemical potential (– 3.04 V vs. SHE), and is very lightweight. [2, 3] However, lithium metal is highly reactive, thus it decomposes liquid electrolytes to form a solid electrolyte interphase (SEI). [4] The SEI is a highly resistive film that causes significant transport resistance during battery operation and consumes lithium and electrolyte during SEI growth. [5] The complex and varied chemical composition and microstructure

of the SEI layer can further exacerbate the heterogeneous deposition of lithium metal, leading to the formation of dead lithium and dendrites. [6, 7] The formation of both dead lithium and dendrites results from heterogeneous deposition at the electrode surface. Dead lithium occurs when lithium metal becomes electrically isolated from the current collector, meaning that it is unable to be used for storing energy and is a primary form of long-term failure. Dendrites form when a spike of metal grows significantly faster than the average deposition velocity and is a primary form of catastrophic failure as dendrites can cause a thermal runaway of the battery. [8, 9]

According to established theory, the main mechanism that causes dendrite initiation at a metal electrode undergoing electrodeposition is the depletion of reactant at the electrode/electrolyte interface. [10] The time for the reactant concentration to become depleted during constant current operation is known as the Sand's time. An analytical solution for the Sand's time was derived from a combination of Fick's and Faraday's laws for binary electrolytes but not accounting for the moving interface due to metal electrodeposition. [11] The theory of Sand's time has been shown to be predictive for dendrite initiation in metals that do not form an SEI. [11–15] Previous investigations have shown poor correlation between the onset of dendrites on lithium metal and the classical Sand's time when using transport parameters measured in the electrolyte. [10, 15–18] Derivations of alternative analytical solutions for predicting the Sand's time have ignored the influence of the SEI, despite the SEI severely inhibiting transport of lithium ions to the electrode surface, causing consistently poor Sand's time predictions when compared to experimental data. [15, 17, 18] The key transport parameters governing diffusion are the reactant concentration and diffusivity of the ion through the medium. Previous investigations have measured these parameters to be multiple orders of magnitude smaller in the SEI when compared to the liquid electrolyte, which is a factor that has not been considered in previous publications on the Sand's time for lithium metal electrodes. [19, 20] Additionally, analytical solutions treat the electrode boundary as stationary when in experiments the electrode grows over time, extending into the electrolyte. A numerical model with a moving boundary can simulate the electrodeposition process more robustly, including the dynamic evolution of the SEI thickness, thus resulting in more accurate prediction of concentration depletion.

Recently, an analytical solution of the Sand's time modified to incorporate the presence of the SEI was published and showed improved correlation with experimental data and that the equation can be reduced to a single fitting parameter. [21] However, a single constant parameter cannot capture the spatiotemporal evolution of the SEI and its effect on Li-ion transport to the reactive surface. To this end, we constructed a 1D numerical model to simulate the simultaneous competing reactions of lithium electrodeposition and SEI growth. The model captures both the moving Li-metal interface due to electrodeposition and the thickening SEI layer that further impedes ion transport over time, resulting in lithium ion depletion at the electrode surface and the initiation of a dendrite. We show that this 1D model is accurate when compared to experimental data and that the sensitivity of the Sand's time to diffusion and electromigration transport parameters is different for low and high applied current density. We then extend the model to two dimensions (2D) to demonstrate the impact of surface heterogeneity on the plating uniformity and chemical potential gradients in the presence of an SEI. We argue that improved characterization of the transport properties of the SEI, including thickness,

limiting concentration, and lithium diffusivity, is necessary for designing electrolytes and artificial SEIs to improve lithium metal electrode stability.

2 Methods

We constructed a one-dimensional (1D) model with a domain that grows as a result of the SEI formation reaction that occurs at the surface of the lithium metal electrode. The objective is to simulate concentration depletion and estimate the Sand's time in the presence of a growing SEI. Given the highly transport-limiting nature of the inorganic layer of the SEI, our model focuses on its growth and transport of Li^+ through it. Transport in the porous organic layer of the SEI and liquid electrolyte is not modeled explicitly, as we found it to be not limiting given the relatively poor transport properties of inorganic layer of the SEI. The modeling domain represents the growing SEI layer, and its dimension increases over time. We imposed a constant current boundary condition at the electrode and constant ionic potential and concentration at the SEI surface (Fig. 1A). The constant current condition caused lithium plating and SEI growth at the electrode surface, thus representing the charge cycle during formation cycling and standard battery operation. The time-dependent mass balance governed the reaction and diffusion of species within the SEI,

$$\frac{\partial c_i}{\partial t} + \nabla \cdot N_i = 0 \tag{1}$$

where c_i was the species concentration, t was time, N_i was the species flux. The Nernst-Planck equation governed the species transport through the SEI,

$$N_i = -D_i \nabla c_i - \frac{z_i F}{RT} D_i c_i \nabla \phi_l \tag{2}$$

where D_i was the diffusivity, and z_i was the charge of species i, F was Faraday's constant, R was the molar gas constant, and T was the temperature (assumed to be a constant

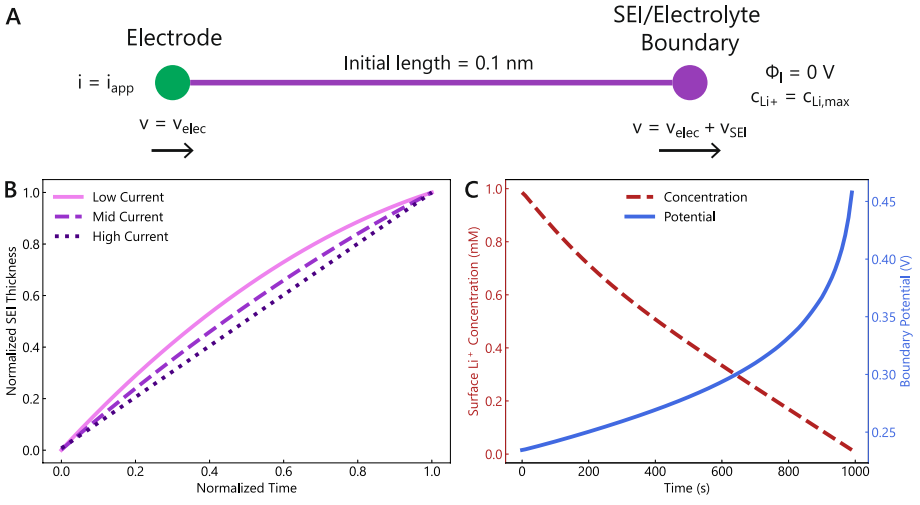

Fig. 1 **A** Schematic of the 1D homogeneous model. **B** Demonstration of the different growth trajectories of the SEI as a function of applied current density. Time and thickness were normalized to the final time and thickness at the end of the simulation. **C** Sample results of the Li^+ concentration at the surface of the electrode and external electric potential

298 K). [22, 23] We modeled the ionic potential using the Poisson equation through the length of the electric field displacement D_l,

$$\nabla \cdot D_l = F \sum_i z_i c_i \tag{3}$$

$$D_l = -\epsilon_0 \epsilon_r \nabla \phi_l \tag{4}$$

where ϵ_0 was the permittivity of free space and ϵ_r was the relative permittivity of the SEI. We found that the permittivity had almost no impact on the Sand's time predictions and little impact on the chemical potential gradient distribution within the SEI. We imposed boundary conditions of ϕ_l = 0 V and $c_i = c_{init}$ at the SEI/electrolyte boundary. Using this model allows for charge separation in the first few nanometers away from the electrode surface, which is necessary for accurate modeling at the nanometer scale. We assumed three species in the electrolyte: Li^+, a generic monovalent anion, and a generic, uncharged solvent molecule.

The initial length of the domain was 0.1 nm, which then grew as the simulation progressed as a result of reaction competition at the electrode. We modeled the electrode as a smooth, planar surface (a single point in 1D) with two competing reactions: lithium plating

$$Li^+ + e^- \rightarrow Li_{(s)} \tag{5}$$

and SEI formation

$$2Li^+ + 2Sol + 2e^- \rightarrow SEI_{(s)} \tag{6}$$

where "Sol" is a solvent molecule. While SEI formation is believed to be a more complex, multistep electroprecipitation process, many continuum models have accurately modeled it as a one-step electrochemical reaction. [24–26] We modeled the lithium deposition kinetics using the concentration-dependent Butler-Volmer equation. For the lithium plating reaction, the local current density was given by the concentration-dependent Butler-Volmer equation,

$$i_{\text{elec}} = i_0 \left[\frac{c_s}{c_{\text{ref}}} \exp\left(\frac{\alpha F \eta}{RT}\right) - \frac{c_s}{c_{\text{ref}}} \exp\left(\frac{(1-\alpha) F \eta}{RT}\right) \right] \tag{7}$$

where i_{elec} was the current density for the plating reaction, i_0 was the exchange current density, c_s is the concentration of lithium ions at the electrode-SEI interface, c_{ref} was the reference concentration (1 M), α was the symmetry factor, and η was the reaction overpotential. For the SEI reaction, the local current density was

$$i_{\text{SEI}} = k_{\text{SEI}} c_{\text{sol}} F \left[\exp\left(\frac{\alpha F \eta}{RT}\right) - \exp\left(\frac{(1-\alpha) F \eta}{RT}\right) \right] \tag{8}$$

where i_{SEI} was the current density for the SEI reaction, k_{SEI} was the SEI reaction rate, and c_{sol} was the concentration of solvent at the surface. We imposed a constant current boundary condition ($i = i_{app}$) at the electrode, and this current was partitioned by the local current densities as a result of the local reactant concentrations, reaction rates, and thus overpotentials.

Boundary growth velocities were calculated as a function of the local reaction rate and the respective growing material. For the plating reaction, we defined the velocity as

$$v_{\mathrm{elec}} = \frac{i_{\mathrm{elec}}}{F\rho_{\mathrm{Li}}} \tag{9}$$

where ρ_{Li} was the molar density of lithium metal. For the SEI reaction, we defined the velocity as

$$v_{\mathrm{SEI}} = \frac{i_{\mathrm{SEI}}}{2F\rho_{\mathrm{SEI}}} \tag{10}$$

where ρ_{SEI} was the molar density of the SEI. Thus, the electrode/SEI boundary (left node in Fig. 1A) moved at $\mathrm{v_{elec}}$ and the right boundary moved at $\mathrm{v_{elec}} + \mathrm{v_{SEI}}$ to capture the effects of both the growth of the surface and the growth of the SEI. The simulation domain, being entirely comprised of SEI, therefore grew in time as a function of the SEI properties and applied current density. The propagation of the electrode boundary is typical in liquid electrolyte systems, but was not found to make a significant different due to the focus on transport through the thin SEI. The equations were compiled and solved in COMSOL Multiphysics 6.3. The resultant SEI growth profiles were as expected: linear for short times/high applied current density and saturated at longer times/low applied current density (Fig. 1B). The model accurately simulated lithium ion concentration depletion at the electrode surface and the resulting exponential increase in the potential at the solid boundary due to the concentration polarization (Fig. 1C). We estimated the Sand's time to be the time when the surface concentration of Li^+ reaches 1 μM, at which point the simulation was stopped. This value was chosen because it is three orders of magnitude below the baseline initial condition for lithium concentration.

Since the native SEI is a heterogeneous material, and we simulated it as homogeneous, we chose baseline parameters for the simulations to be average representations of SEI properties (Table 1). Of significance was the limit of lithium concentration imposed within the domain to 1 mM, which has been previously measured to be within this order of magnitude. [19, 20]

3 Results

3.1 Comparison to experimental data

Previous experimental literature has estimated the Sand's time for lithium metal for a range of applied current densities using a combination of optical and electrochemical

Table 1 Baseline non-lithium transport parameters used in base 1D model for estimating the Sand's time

Name	Variable	Value
Anion diffusivity	D_{An}	$1 \times 10^{-13} m^2 s^{-1}$
Solvent diffusivity	D_{sol}	$1 \times 10^{-15} m^2 s^{-1}$
SEI permittivity	ϵ_r	10
Li plating exchange current density	i_0	$10\, Am^{-2}$
Symmetry factor	α	0.5
SEI reaction rate	k_{SEI}	$5 \times 10^{-17} s^{-1}$
Initial solvent concentration	c_{sol}	4.5 M
Lithium metal molar density	ρ_{Li}	76801 $mol m^{-3}$
SEI molar density	ρ_{SEI}	28552 $mol m^{-3}$

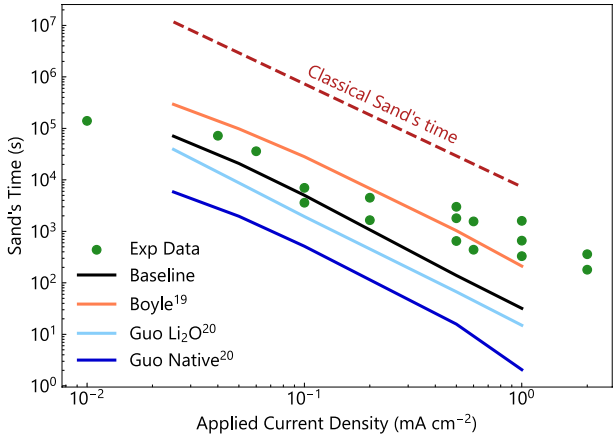

Fig. 2 Comparison of experimental data [27–32] to model results using the baseline parameters, and values for the maximum Li^+ concentration and Li^+ diffusivity from Boyle et al. and Guo et al. [19, 20]

Table 2 Baseline and alternative limiting concentration and diffusivities from literature [19, 20]

Name	Concentration limit (mM)	Diffusivity ($m^2 s^{-1}$)
Baseline	1.0	1.0×10^{-13}
Boyle et al	2.1	2.2×10^{-13}
Guo et al. Li_2O	0.3	1.8×10^{-13}
Guo et al. native SEI	9.0	1.8×10^{-15}

data. [10, 27–32] Our model was shown to accurately predict the Sand's time, with better accuracy at low applied current density when using the baseline parameters (Fig. 2), which was consistent with the long-term SEI growth model used. There is a larger variance in the experimental data at high applied current density, indicating that the properties of the SEI heavily influence the Sand's time. The experimental data has a slope of −1.4, while the numerical results have a slope of −1.9, which was insensitive to the parameters used. However, this slope aligns well at low applied current density and poorly at high applied current density, possibly suggesting different phenomena for these two regimes. These results could be explained by different SEI components growing over time, with the phases that grow quickly having better transport properties than the phases that take longer to form.

Previous publications have measured the lithium concentration limit and lithium diffusivity within a native SEI and thin-film lithium oxide (Table 2). The measurements from Boyle et al. [19] shift the Sand's time prediction to larger values due to both parameters being higher than the baseline, thus increasing the accuracy at high applied current density and decreasing the accuracy at low applied current density. The measurements from Guo et al. [20] for the native SEI and Li_2O showed the extremes of increasing each parameter above the baseline, with the diffusivity and maximum concentration of each material being either well above or below the baseline. The results using the native SEI parameters from Guo et al. were the closest to the slope of the experimental data, with other parameter sets generally being too steep (model is ∼−1.9 while the experimental data is ∼−1.4). While it is clear that the Sand's time is highly sensitive to the SEI transport properties it is difficult to fit both low and high current data with the same set of parameters.

While there is variance in the experimental data making it difficult to fit a model precisely, there are also gaps in fundamental knowledge that inhibit our ability to create an accurate model. First, the material composition of the SEI and how it evolves over time is highly dependent upon the electrolyte components and electrochemical conditions to which the battery has been subjected. There are many theories that discuss how the growth of the different phases (crystalline vs. amorphous, organic vs. inorganic, etc.) evolve over time, but definitive knowledge of this evolution is still not present in literature, inhibiting our ability to create accurate growth models and assign kinetic rates to different phases. [24, 33] Additionally, characterization and parameterization of the different phases is poor, thus knowledge of critical values of transport parameters such as diffusivity, maximum concentration, porosity, and thickness are lacking. Second, the reaction competition between plating and SEI growth has recently been shown to be dependent on the applied current density and facet upon which the lithium plates. [34] The model can account for SEI properties that depend or evolve with electrochemical conditions and time. With greater knowledge of this phenomenon, models will be able to better predict dendrite initiation over a larger range of applied current densities. We assert that deeper characterization of the SEI is needed to more accurately predict the Sand's time and therefore the initiation of dendrites. Many strong advances are being made using techniques such as cryo-electron microscopy and synchrotron-enhanced surface characterization to quantify SEI thickness and identify specific components of the film. [35, 36] Continuing to deepen our understanding of the SEI material properties will enable the engineering of native and artificial SEIs to improve the stability of lithium metal electrodes for all electrochemical applications.

3.2 Sensitivity to SEI properties

Because a longer Sand's time is desired for greater stability, it becomes pertinent to understand how the properties of the SEI can influence the Sand's time. In the model, there are three main parameters that impact the Sand's time prediction: SEI growth rate, maximum lithium concentration, and lithium diffusivity, which we varied systematically to better understand their impact on dendrite formation. The SEI growth rate is an independent parameter from the other two, and it dictates the size of the domain and therefore the distance through which lithium must diffuse. As is intuitive, faster SEI growth rates resulted in shorter Sand's times (Fig. 3A). Since the SEI has poor transport properties, the faster it grows, the sooner there will be significant concentration depletion at the electrode surface. Thus, our model shows that having a slower growing SEI is beneficial for preventing dendrites and promoting homogeneous lithium plating, as is consistent with previous literature.

The maximum lithium concentration and lithium diffusivity are parameters more directly related to transport, and they are also in the original Sand's time analytical solution. To analyze the sensitivity of the Sand's time to these parameters, we swept them an order of magnitude above and below the baseline parameters for low to medium applied current densities (0.025 to 1 mA cm^{-2}). Below the baseline values, there was a very similar response of the Sand's time to poorer max concentration and diffusivity (Fig. 3B and C). Above the baseline values, there were appreciable differences in the response of the Sand's time to increasing the parameter values. Increasing diffusivity had an almost linear relationship with the Sand's time at low applied current density; a 5x increase in

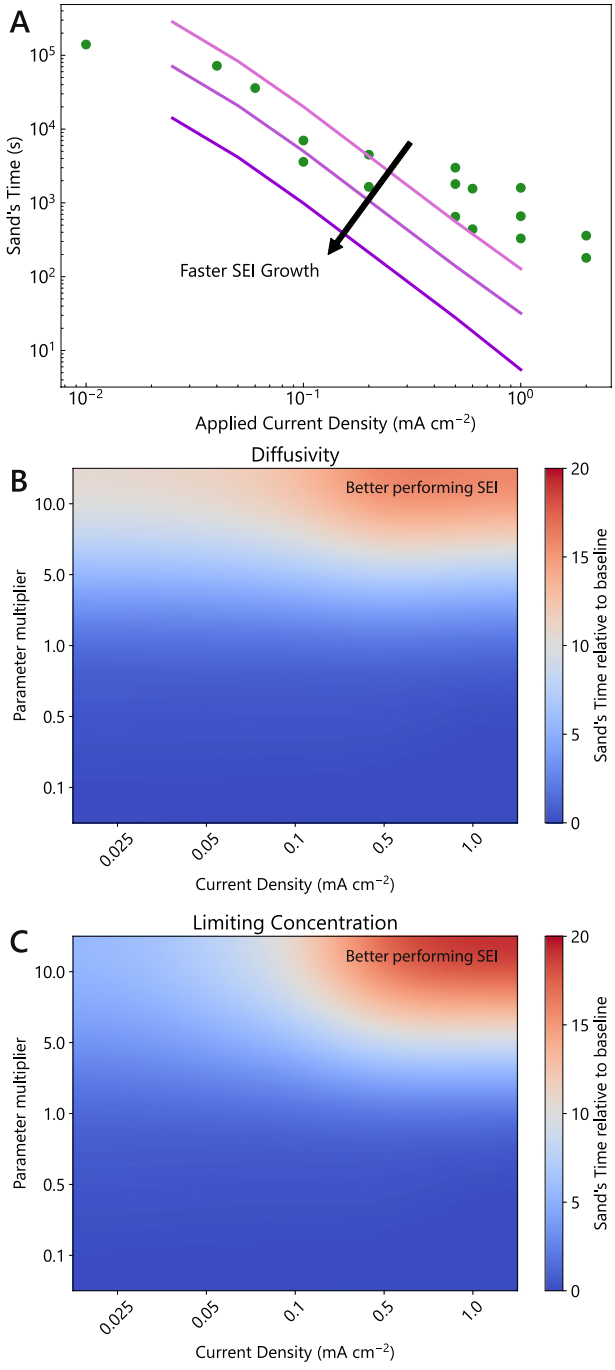

Fig. 3 Sensitivity of the Sand's time to **A** SEI growth rate, **B** diffusivity, and **C** limiting concentration for a range of applied current densities. Y-axes in (**B**) and (**C**) are linear in scale. Parameter multiplier in (**B**) and (**C**) refers to the scalar applied to the variable of interest to conduct the sensitivity analysis

diffusivity increased the Sand's time by ∼5x below 0.1 mA cm^{-2}. At higher current densities, the Sand's time response was larger, with the increase in Sand's time being larger than the increase in the diffusivity. On the other hand, increasing the limiting concentration mattered less at low applied current and more at the higher currents simulated. At an applied current of 1 mA cm^{-2}, increasing the limiting concentration by 10x resulted in a Sand's time that was 20 times that of the baseline. These results demonstrate the

impact of how targeting specific material properties can be more beneficial for certain applications.

3.3 Contributions to chemical potential gradient

While dendrite formation is caused by concentration depletion, the transport of lithium to the electrode surface is a combination of diffusion and electromigration, as is shown by the Nernst-Planck equation (Eq. (2)). Diffusion is governed by the concentration gradient, dc/dx, and electromigration by the electrolyte potential gradient, $d\phi/dx$. To directly compare these two gradients, we normalized them to the chemical potential gradients. We calculated the diffusive chemical potential gradient as

$$\frac{d\mu_{\text{diff}}}{dx} = \frac{dc}{dx}\frac{RT}{c_{\max}} \tag{11}$$

and the electromigration chemical potential gradient as

$$\frac{d\mu_{\text{mig}}}{dx} = \frac{d\phi}{dx}F \tag{12}$$

We present the results for the two components of the chemical potential gradient through the SEI at the last time step of the simulations. We compare the diffusive and electrostatic driving forces on the ion transport and the onset of dendrite formation. We note that nondimensionalizing the contributions to lithium flux yields the same trends but with different raw values.

In all cases, the electromigration chemical potential gradient asymptotes to zero at the electrode/SEI interface (Fig. 4). The asymptote appears to be a result of the simulations being in 1D, for which we present further justification and discussion later in the manuscript. At high applied current density, the diffusive chemical potential gradient dominated over electromigration (Fig. 4A). At a current density of 0.5 mA cm^{-2}, the diffusive chemical potential gradient was $\sim 10^{12}$ J mol^{-1} m^{-1} while electromigration increased from 10^{10} to 10^{11} when going through the SEI from the electrode to the electrolyte. As the current density decreased, the two chemical potential gradients were similar orders of magnitude throughout the thickness of the SEI. For a current density of 0.05 mA cm^{-2}, the electromigration contribution was larger than the diffusive contribution for 80% of the SEI. This result is somewhat counterintuitive because it could be expected that higher current would produce larger potential gradients due to the higher overpotential at the electrode surface. Instead, the higher applied current and increased rate of consumption created a strong concentration gradient, causing the diffusive chemical potential gradient to be much higher.

Poorer SEI properties – low limiting concentration and diffusivity – resulted in the diffusive chemical potential gradient being several orders of magnitude larger than electromigration (Fig. 4B and C). For a limiting concentration of 0.1 mol m^{-3}, the diffusive chemical potential gradient was $\sim 2.5 \cdot 10^{12}$ J mol^{-1} m^{-1} and the electromigration gradient was never above 3 x 10^{9} J mol^{-1} m^{-1}. Similarly for a diffusivity of 1 x 10^{-14} m^2 s^{-1}, the diffusive chemical potential gradient was ~2.5 x 10^{12} J mol^{-1} m^{-1} and the electromigration gradient peaked at 4 x 10^{10} J mol^{-1} m^{-1}. However, for better SEI properties – high limiting concentration and diffusivity – the electromigration chemical potential gradient was greater than diffusive for almost the entire SEI thickness. For low

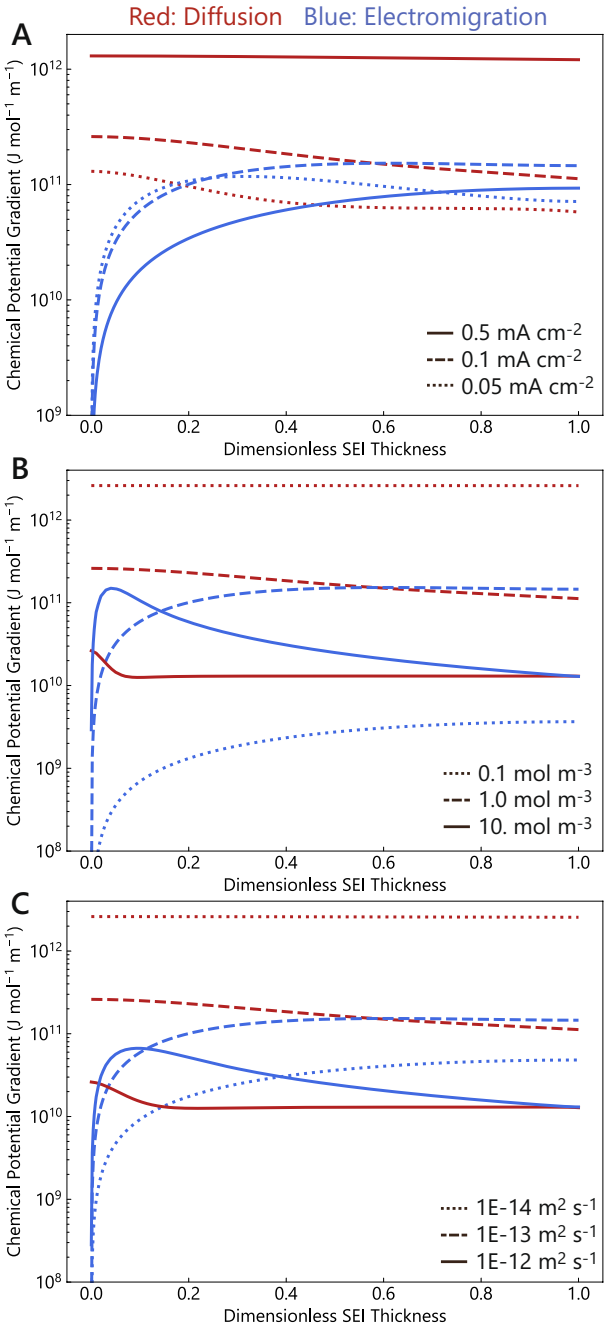

Fig. 4 Contributions to the chemical potential gradient from diffusion (red) and electromigration (blue) for different **A** current densities, **B** maximum Li^+ concentration, and **C** Li^+ diffusivities

limiting concentration and diffusivity, the electromigration chemical potential gradient was at its maximum at the SEI/electrolyte interface. However, for c_{max} = 10 mol m^{-3} and D_{Li} = 10^{-12} m^2 s^{-1}, there was a peak in the electromigration chemical potential gradient approximately 5-10% of the depth into the SEI thickness, decaying back down to being equal to that of the diffusive chemical potential gradient. Overall, this demonstrates that a better performing SEI minimizes concentration gradients. These SEI properties are similar to ceramic solid state electrolytes with high transference numbers, with lithium flux being driven by electromigration.

3.4 Analysis of 2D protrusion

The previously presented work was in 1D, assuming a perfectly flat electrode, which is rarely the case. Inhomogeneity at the electrode surface can be as a result of a rough current collector, lithium nuclei deposited in various sized islands, or a dendrite that has begun forming from overlimiting current. To investigate the impact of roughness, we created a two-dimensional (2D) domain 10 x 10 nm in size to simulate a fixed-thickness SEI (Fig. 5A). The same equations were used for the 2D simulations, with the simplification that there is no longer a reaction competition at the electrode, thus we are assuming that the SEI is fully saturated. In the 2D simulations, there is only the lithium deposition reaction at the electrode boundary, and the opposite boundary moves at the average velocity of the electrode, preserving the domain size for the simulation. While the SEI is not growing over the course of the simulations, its role is to add a transport barrier for Li-ions to reach the reducing surface. We set the maximum concentration of lithium in the domain to 1 mM and the Li^+ diffusivity to $10^{-13}\ m^2\ s^{-1}$, each three orders of magnitude lower than what is typically measured in a liquid electrolyte. We implemented symmetry boundary conditions at the walls to ensure that the distortion of the electric field lines only result from the heterogeneity of the electrodeposition. At a physical electrode, the mechanical forces present within the SEI and at the electrode/SEI interface would impact the long-term growth of a dendrite during electrochemical cycling of the electrode. This work does not consider the impact of mechanical forces due to the

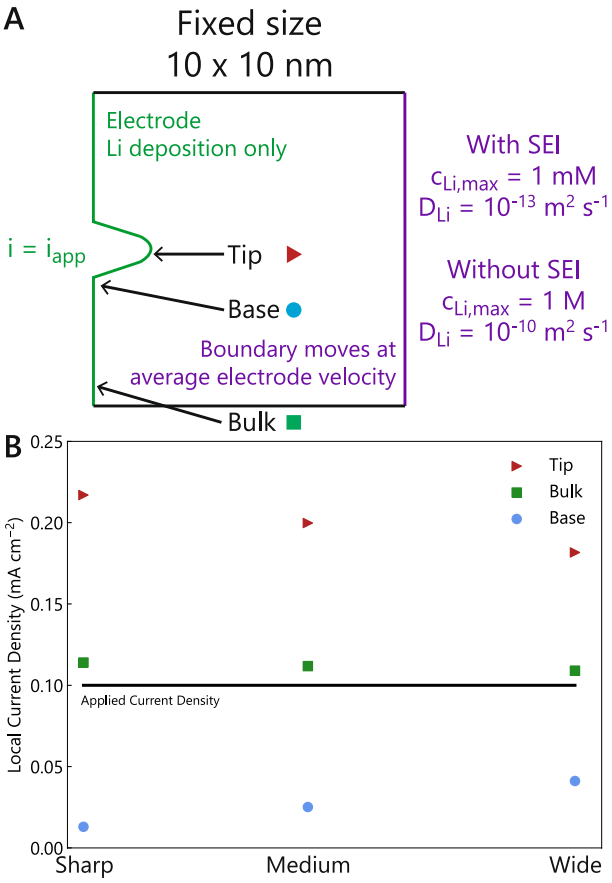

Fig. 5 **A** Schematic of simulation domain for 2D protrusion simulations. **B** Local current density for three different locations along the electrode for different curvatures of protrusion covered by a 10 nm SEI

difference in time scales over which dendrite formation and mechanical stresses occur and the additional physics that would be required in the model to couple chemomechanics and transport. The purpose of the 2D analysis is to understand how the presence of the SEI resistive layer affects the evolution of the Li interface. The SEI may exacerbate instabilities, in the Li-deposition process, by enhancing concentration gradients along the interface.

We created a protrusion on the electrode to simulate a small section of a rough surface on the electrode. We varied the shape of the protrusion, with a "wide" shape being 2 nm wide and 0.5 nm tall (into the SEI) with a curvature of 0.36 nm^{-1}, a "medium" shape being 1.7 nm wide and 0.75 nm tall with a curvature of 1.78 nm^{-1}, and a "sharp" shape being 1 nm wide and 1 nm tall with a curvature of 3.0 nm^{-1}. The total surface length of the protrusion was kept constant between all three shapes to ensure fair comparison of surface area between the designs. This scale of protrusion has been previously measured at copper current collectors and lithium metal anodes, showing that different levels of roughness significantly impact battery performance due to morphological stability. [37]

Along the length of the electrode, inhomogeneity creates variation in the local current density, and the variation is exacerbated due to the presence of the SEI. In our model, as the protrusion became sharper, the variation in local current density became larger (Fig. 5B). For the sharp protrusion, the current at the tip was 117% greater than the applied current density (0.1 mA cm^{-2}) and the current at the base of the protrusion was 13% of the applied current density. For the wide protrusion, the current density at the tip was 0.18 mA cm^{-2} and 0.04 mA cm^{-2} at the base. Since the tip is quite small, the Gibbs-Thomson effect would be considerable, but this effect would only occur at the very tip of the protrusion and decay rapidly down the walls of the protrusion. [38] Thus, the non-uniform current would still be produced due to the severe transport limitations imposed by the SEI. These results emphasize the importance of smooth current collectors and electrodes in lithium metal devices.

The variation in local current density caused the protrusion to become more inhomogeneous over time when the SEI was present (Fig. 6). As the tip of the protrusion became sharper and the curvature larger, the deposition profile became worse. For the wide protrusion, the shape stayed relatively constant during deposition, with the distance between the base and the tip growing from 0.5 to 0.75 nm (Fig. 6A). On the other hand, for the sharp protrusion, the protrusion changed much more dramatically, with the distance between the base and the tip growing from 1 to 1.7 nm (Fig. 6C). Additionally, the shape of the protrusion changed, with the thickness of the dendrite becoming wider over time, which would likely cause a cascading effect of continuing to make the deposition profile worse. By modifying the transport parameters to be more representative of the electrolyte (concentration = 1 M; diffusivity = 10^{-10} m^2 s^{-1}), the deposition profile became extremely uniform, even for the sharp protrusion (Fig. 6D). This demonstrates the importance of an SEI with good transport parameters and indicates that the mechanism of dendrite formation with an SEI is not necessarily the same as without an SEI.

Previously, we demonstrated the variation in chemical potential gradients in one dimension (1D). In two dimensions (2D), the presence of a protrusion introduces additional variation in the chemical potential gradients within the SEI, due to its sluggish transport properties. Away from the protrusion, toward the bulk of the electrode surface,

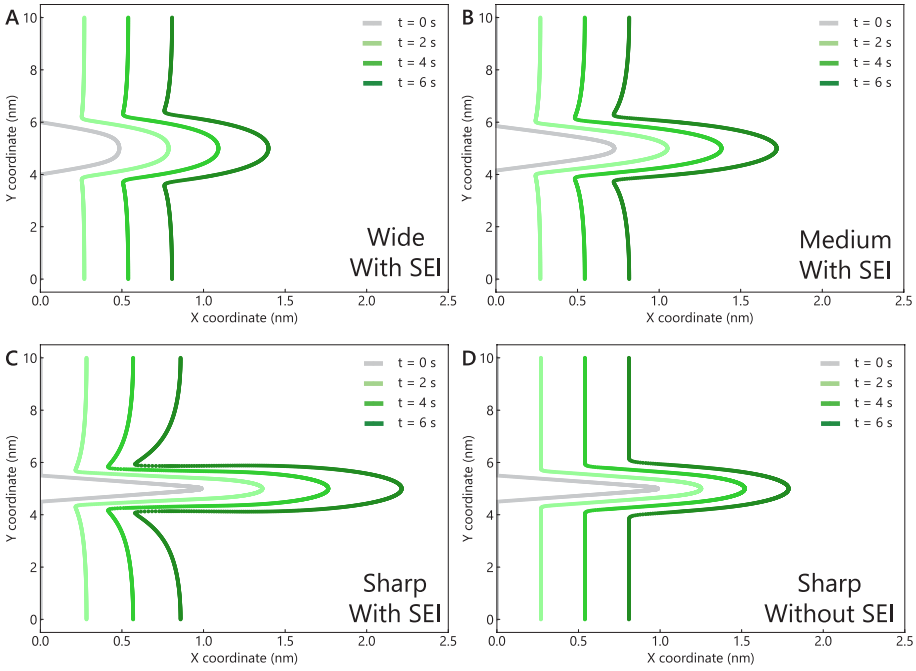

Fig. 6 Evolution of the electrode boundary over the first 6 s of deposition at 0.1 mA cm^{-2} for different curvature of protrusions and with and without an SEI layer present

the 2D chemical potential gradients resemble those observed in the 1D case with the SEI present (Fig. 7A and C).

With the SEI, a hotspot in the diffusive chemical potential gradient appears at the tip of the protrusion, diminishing toward the base and further away from the defect. The minimum diffusive gradient occurs at the base of the protrusion, where both the concentration and its gradient are low, likely a result of reduced local current density. As in the 1D case, the minimum electromigration gradient is found at the electrode surface, except at the sides of the protrusion, where the gradient reaches approximately $\sim$8 x 10^{10} J mol^{-1} m^{-1}. This elevated electromigration at the protrusion sides may enhance lithium flux to the electrode, partially homogenizing the current and extending the time before lithium is depleted at the surface.

Similar to the 1D scenario, the magnitudes of the chemical potential gradients from diffusion and electromigration are comparable away from the electrode surface, but diffusion dominates at the surface (Fig. 7A and C). The SEI increases the magnitude of the chemical potential gradient by factors of 10^3 and 10^6 for the electrostatic and diffusive components, respectively, compared to the case without the SEI (Fig. 7B and D). Without the SEI, the chemical potential gradients are distributed much more uniformly along the electrode surface and through the first 10 nm of the electrolyte. Thus, the SEI amplifies the gradients along the interface, accelerating protrusion growth. Overall, these results show that the presence of the SEI exacerbates issues with lithium flux to the surface, creating hotspots and increasing gradients that contribute to electrode instability and propensity of dendrite formation and growth.

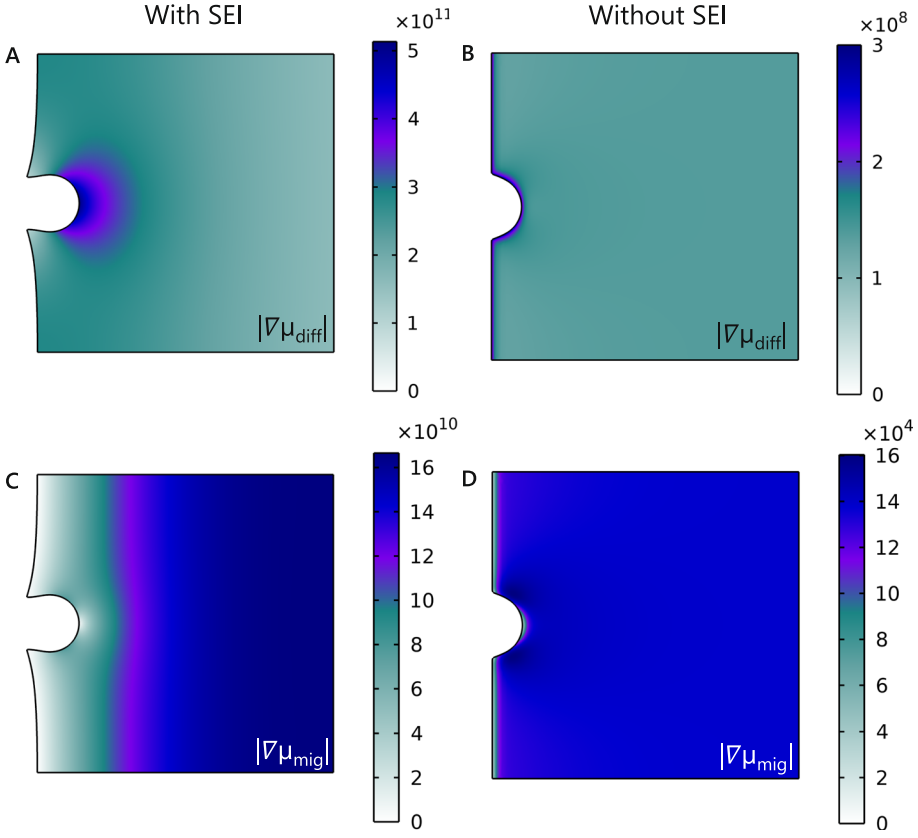

Fig. 7 Diffusion and electromigration chemical potential gradients around the protrusion and through the 10 nm SEI (**A**) and (**C**) and electrolyte (**B**) and (**D**). Contours taken at t = 6 s with an applied current density of 0.1 $mA\,cm^{-2}$ for the sharp protrusion. All results have units of $J\,mol^{-1}m^{-1}$

4 Conclusions

We demonstrated that the Sand's time can be more accurately predicted by simulating only the solid electrolyte interphase (SEI). The Sand's time and dendrite formation are thus highly sensitive to the thickness and transport parameters of the SEI layer, specifically the maximum lithium concentration and diffusivity. We found that an SEI with better transport properties decreased the diffusion chemical potential gradient and increased the electromigration chemical potential gradient, providing insight into desirable properties of the SEI. For instance, an artificial SEI layer with a transference number approaching one would be favorable for reducing ion depletion and delaying the diffusion limited conditions represented by the Sand's time. 2D modeling results showed that the presence of an SEI on a rough surface increased plating non-uniformity due to larger variations in local current densities. The effect is more severe for sharper protrusions. Additionally, the SEI caused an increase in the chemical potential gradients, thus creating hotspots at the tip of the dendrite, and further exacerbating transport issues. These results demonstrate that more detailed characterization of the SEI is needed to better understand the transport phenomena through the SEI and design higher performing electrolytes and artificial SEI layers.

Acknowledgements
There are no additional people to acknowledge.

Author contributions
Conceptualization—NRC, TYL, RA, CO, GB; Methodology—NRC, TYL, NWB, VME, RA, CO, GB; Analysis – NRC, TYL, NWB, SSS, VME, TR, HL, RA, MAW, CO, GB; Visualization—NRC, TYL, TR, GB; Writing—NRC, GB; Reviewing and Editing—NRC, TYL, NWB, SSS, VME, TR, HL, RA, MAW, CO, GB

Funding
This work was performed under the auspices of the U.S. Department of Energy by Lawrence Livermore National Laboratory under Contract DE-AC52-07NA27344. This work was supported by the Lawrence Livermore National Laboratory LDRD 23-SI-002. LLNL release number LLNL-JRNL-2008837.

Data availability
The data from the current study are available from the corresponding author with reasonable request.

Declarations

Ethics approval and consent to participate
Not applicable.

Consent for publication
Not applicable.

Competing interests
The authors declare no competing interests.

Received: 6 August 2025 / Accepted: 6 February 2026
Published online: 16 February 2026

References

1. Jones K, Ginley D. Materials for electrification of everything: moving toward sustainability. MRS Bull. 2021;46(12):1130–8.
2. M. Stanley Whittingham. History, evolution, and future status of energy storage. *Proceedings of the IEEE*, 100(Special Centennial Issue):1518–1534, 2012. https://doi.org/10.1109/JPROC.2012.2190170.
3. Lewis GN, Keyes FG. The potential of the lithium electrode. J Am Chem Soc. 1913;35(4):340–4.
4. Peled E. The electrochemical behavior of alkali and alkaline earth metals in nonaqueous battery systems-the solid electrolyte interphase model. J Electrochem Soc. 1979;126(12):2047.
5. Peled E, Menkin S. Sei: past, present and future. J Electrochem Soc. 2017;164(7):A1703.
6. Abdollahifar M, Paolella A. "Dead lithium" formation and mitigation strategies in anode-free Li-metal batteries. Batteries Supercaps. 2025;8(3):e202400505.
7. Jiang Y, Ye F. Dead lithium in lithium metal batteries: formation, characterization and strategies. Chem-A Eur J. 2024;30(43):e202400424.
8. Cui X, Wang J, Sun S, Chen X, Wang Y, Han D, et al. Safety hazards of lithium metal batteries: from the perspective of lithium dendrites and thermal runaway. Energy Fuels. 2025;39(16):7665–90.
9. Zhang S, Shen Z, Yingying L, et al. Research progress of thermal runaway and safety for lithium metal batteries. Acta Phys Chim Sin. 2021;37(1):2008065.
10. Peng Bai J, Li FRB, Bazant MZ. Transition of lithium growth mechanisms in liquid electrolytes. Energy Environ Sci. 2016;9(10):3221–9.
11. Sand HJS. On the concentration at the electrodes in a solution, with special reference to the liberation of hydrogen by electrolysis of a mixture of copper sulphate and sulphuric acid. Proc Phys Soc Lond. 1899;17(1):496. https://doi.org/10.1088/1478-7814/17/1/332.
12. Zhang J, Huang W, Li L, Chang C, Yang K, Gao L, et al. Nonepitaxial electrodeposition of (002)-textured Zn anode on textureless substrates for dendrite-free and hydrogen evolution-suppressed Zn batteries. Adv Mater. 2023;35(21):2300073. https://doi.org/10.1002/adma.202300073.
13. Argoul F, Freysz E, Kuhn A, Léger C, Potin L. Interferometric characterization of growth dynamics during dendritic electrodeposition of zinc. Phys Rev E. 1996;53:1777–88. https://doi.org/10.1103/PhysRevE.53.1777.
14. Rosso M, Chassaing E, Chazalviel J-N. Role of buoyancy in the onset of dendritic growth in thin layer electrodeposition. Phys Rev E. 1999;59:3135–9. https://doi.org/10.1103/PhysRevE.59.3135.
15. Yang P. Dendrite growth on metal anodes: a unified framework bridging diffusion and interfacial kinetics. ACS Energy Lett. 2025;10(10):5040–6. https://doi.org/10.1021/acsenergylett.5c02663.
16. Wasalathanthri RN, Akolkar R. Perspective-does the sand equation reliably predict the onset of morphological evolution in lithium electrodeposition? J Electrochem Soc. 2022;169(9):092519.
17. Hoffman ZJ, Mistry A, Srinivasan V, Balsara NP. Comparing experimentally-measured sand's times with concentrated solution theory predictions in a polymer electrolyte. J Electrochem Soc. 2023;170(12):120524.
18. Lee Y, Ma B, Bai P. Overlimiting ion transport dynamic toward sand's time in solid polymer electrolytes. Materials Today Energy. 2022;27:101037.
19. Boyle DT, Li Y, Pei A, Vilá RA, Zhang Z, Sayavong P, et al. Resolving current-dependent regimes of electroplating mechanisms for fast charging lithium metal anodes. Nano Lett. 2022;22(20):8224–32. https://doi.org/10.1021/acs.nanolett.2c02792.
20. Guo R, Gallant BM. Li2o solid electrolyte interphase: probing transport properties at the chemical potential of lithium. Chem Mater. 2020;32(13):5525–33. https://doi.org/10.1021/acs.chemmater.0c00333.
21. Ma Y, Selvasundarasekar SS, Sinclair N, Zhang Y, Shaomao X, Bracey J, et al. A modified sand's time incorporating Li-ion transport across the sei: basis for understanding Li dendrite formation and li-metal battery electrolyte selection. J Electrochem Soc. 2025;172(3):030506.

22. Christensen J, Newman J. A mathematical model for the lithium-ion negative electrode solid electrolyte interphase. J Electrochem Soc. 2004;151(11):A1977.
23. Liu G, Wei L. A model of concurrent lithium dendrite growth, sei growth, sei penetration and regrowth. J Electrochem Soc. 2017;164(9):A1826.
24. Wang A, Kadam S, Li H, Shi S, Qi Y. Review on modeling of the anode solid electrolyte interphase (sei) for lithium-ion batteries. NPJ Comput Mater. 2018;4(1):15.
25. Weng A, Olide E, Kovalchuk I, Siegel JB, Stefanopoulou A. Modeling battery formation: boosted sei growth, multi-species reactions, and irreversible expansion. J Electrochem Soc. 2023;170(9):090523. https://doi.org/10.1149/1945-7111/aceffe.
26. MadiReddy SK, Shang W, White RE. Mathematical model for sei growth under open-circuit conditions. J Electrochem Soc. 2022;169(9):090505. https://doi.org/10.1149/1945-7111/ac8ee5.
27. Fei Ding WX, Graff GL, Zhang J, Sushko ML, Chen X, Shao Y, et al. Dendrite-free lithium deposition via self-healing electrostatic shield mechanism. J Am Chem Soc. 2013;135(11):4450–6.
28. Maraschky A, Akolkar R. Mechanism explaining the onset time of dendritic lithium electrodeposition via considerations of the li^+ transport within the solid electrolyte interphase. J Electrochem Soc. 2018;165(14):D696.
29. Crowther O, West AC. Effect of electrolyte composition on lithium dendrite growth. J Electrochem Soc. 2008;155(11):A806.
30. Yingying L, Zhengyuan T, Archer LA. Stable lithium electrodeposition in liquid and nanoporous solid electrolytes. Nat Mater. 2014;13(10):961–9.
31. Li W, Yao H, Yan K, Zheng G, Liang Z, Chiang Y-M, et al. The synergetic effect of lithium polysulfide and lithium nitrate to prevent lithium dendrite growth. Nat Commun. 2015;6(1):7436.
32. Nishikawa K, Mori T, Nishida T, Fukunaka Y, Rosso M, Homma T. In situ observation of dendrite growth of electrodeposited Li metal. J Electrochem Soc. 2010;157(11):A1212.
33. Horstmann B, Single F, Latz A. Review on multi-scale models of solid-electrolyte interphase formation. Curr Opin Electrochem. 2019;13:61–9.
34. Yuan X, Liu B, Mecklenburg M, Li Y. Ultrafast deposition of faceted lithium polyhedra by outpacing sei formation. Nature. 2023;620(7972):86–91.
35. Dopilka A, Larson JM, Kostecki R. Operando infrared nanospectroscopy of the silicon/electrolyte interface during initial stages of solid-electrolyte-interphase layer formation. ACS Energy Lett. 2024;10(1):410–9.
36. Wang C, Kim JT, Yuan X, Kim JK, Liu B, Kim M, et al. Trapping and imaging dynamic battery nanointerfaces via electrified cryo-EM. Sci Adv. 2025;11(24):eadv3191.
37. Jang T, Kang J-H, Kim S, Shim M, Lee J, Song J, et al. Nanometer-scale surface roughness of a 3-d Cu substrate promoting Li nucleation in Li-metal batteries. ACS Appl Energy Mater. 2021;4(3):2644–51.
38. Akolkar R. Modeling dendrite growth during lithium electrodeposition at sub-ambient temperature. J Power Sources. 2014;246:84–9.